Myeloid calcifying cells promote atherosclerotic calcification via paracrine activity and allograft inflammatory factor-1 overexpression

Albiero, Mattia ; Rattazzi, Marcello ; Menegazzo, Lisa ; Boscaro, Elisa ; Cappellari, Roberta ; Pagnin, Elisa ; Bertacco, Elisa ; Poncina, Nicol ; Dyar, Kenneth ; Ciciliot, Stefano ; Iwabuchi, Kazuya ; Millioni, Renato ; Arrigoni, Giorgio ; Kraenkel, Nicolle ; Landmesser, Ulf ; Agostini, Carlo ; Avogaro, Angelo ; Fadini, Gian Paolo

Abstract: Several cell types contribute to atherosclerotic calcification. Myeloid calcifying cells (MCCs) are monocytes expressing osteocalcin (OC) and bone alkaline phosphatase (BAP). Herein, we tested whether MCCs promote atherosclerotic calcification in vivo. We show that the murine spleen contains OC(+)BAP(+) cells with a phenotype similar to human MCCs, a high expression of adhesion molecules and CD11b, and capacity to calcify in vitro and in vivo. Injection of GFP(+) OC(+)BAP(+) cells into 8- or 40-week ApoE(-/-) mice led to more extensive calcifications in atherosclerotic areas after 24 or 4 weeks, respectively, compared to control OC(-)BAP(-) cells. Despite that OC(+)BAP(+) cells had a selective transendothelial migration capacity, tracking of the GFP signal revealed that presence of injected cells within atherosclerotic areas was an extremely rare event and so GFP mRNA was undetectable by qPCR of lesion extracts. By converse, injected OC(+)BAP(+) cells persisted in the bloodstream and bone marrow up to 24 weeks, suggesting a paracrine effect. Indeed, OC(+)BAP(+) cell-conditioned medium (CM) promoted calcification by cultured vascular smooth muscle cells (VSMC) more than CM from OC(-)BAP(-) cells. A genomic and proteomic investigation of MCCs identified allograft inflammatory factor (AIF)-1 as a potential candidate of this paracrine activity. AIF-1 stimulated VSMC calcification in vitro and monocyte-specific (CD11b-driven) AIF-1 overexpression in ApoE(-/-) mice increased calcium content in atherosclerotic areas. In conclusion, we show that murine OC(+)BAP(+) cells correspond to human MCCs and promote atherosclerotic calcification in ApoE(-/-) mice, through paracrine activity and modulation of resident cells by AIF-1 overexpression.

DOI: https://doi.org/10.1007/s00395-013-0368-7

Myeloid Calcifying Cells Promote Atherosclerotic Calcification via Paracrine Activity and Allograft Inflammatory Factor-1 Overexpression

Authors Mattia Albiero[1], Marcello Rattazzi[2], Lisa Menegazzo[1,2], Elisa Boscaro[1], Roberta Cappellari[2], Elisa Pagnin[2], Elisa Bertacco[2], Nicol Poncina[1,2], Kenneth Dyar[1], Stefano Ciciliot[1,2], Kazuya Iwabuchi[3], Renato Millioni[4], Giorgio Arrigoni[4,5], Nicolle Kraenkel[6,7], Ulf Landmesser[6,7], Carlo Agostini[1,2], Angelo Avogaro[1,2], Gian Paolo Fadini[1,2]

Affiliations [1] Venetian Institute of Molecular Medicine, Padova, Italy.
[2] Department of Medicine, University of Padova, Padova, Italy.
[3] Department of Immunology, Kitasato School of Medicine, Japan.
[4] Proteomic Center of Padova University, Padova, Italy.
[5] Department of Biomedical Sciences, University of Padova, Padova, Italy.
[6] Institute of Physiology, Cardiovascular Research, University of Zurich, Zürich, Switzerland.
[7] University Hospital Zurich, Department of Cardiology, Zürich, Switzerland

Corresponding author
Gian Paolo Fadini
Assistant Professor of Endocrinology and Metabolism
Department of Medicine, University Hospital of Padova
Via Giustiniani, 2. 35100 Padova (Italy).
Phone: 0039-049-8214318; Fax: 0039-049-821-2184
gianpaolo.fadini@unipd.it; gianpaolofadini@hotmail.com

ABSTRACT

Several cell types contribute to atherosclerotic calcification. Myeloid calcifying cells (MCCs) are monocytes expressing osteocalcin (OC) and bone alkaline phosphatase (BAP). Herein, we tested whether MCCs promote atherosclerotic calcification in vivo. We show that the murine spleen contains OC^+BAP^+ cells with a phenotype similar to human MCCs, a high expression of adhesion molecules and CD11b, and capacity to calcify in vitro and in vivo. Injection of GFP^+ OC^+BAP^+ cells into 8- or 40-week $ApoE^{-/-}$ mice led to more extensive calcifications in atherosclerotic areas after 24 or 4 weeks, respectively, compared to control OC^-BAP^- cells. Despite OC^+BAP^+ cells had a selective transendothelial migration capacity, tracking of the GFP signal revealed that presence of injected cells within atherosclerotic areas was an extremely rare event and GFP mRNA was undetectable by qPCR of lesion extracts. By converse, injected OC^+BAP^+ cells persisted in the bloodstream and bone marrow up to 24 weeks, suggesting a paracrine effect. Indeed, OC^+BAP^+ cell conditioned medium (CM) promoted calcification by cultured vascular smooth muscle cells (VSMC) more than CM from OC^-BAP^- cells. A genomic and proteomic investigation of MCCs identified allograft inflammatory factor (AIF)-1 as a potential candidate of this paracrine activity. AIF-1 stimulated VSMC calcification in vitro and monocyte-specific (CD11b-driven) AIF-1 overexpression in $ApoE^{-/-}$ mice increased calcium content in atherosclerotic areas. In conclusion, we show that murine OC^+BAP^+ cells correspond to human MCCs and promote atherosclerotic calcification in $ApoE^{-/-}$ mice, through paracrine activity and modulation of resident cells by AIF-1 overexpression.

Keywords: monocytes; plaques; smooth muscle cells.

INTRODUCTION

Atherosclerosis is a complex inflammatory disease of the artery wall [10]. Ectopic calcification is a common feature of advanced atherosclerotic plaques and it affects vascular function [2]. While extensively calcified lesions may be more stable than lipid-rich lesions, spotty neointimal calcifications are believed to increase lesion vulnerability and probability of rupture [23, 26]. The mechanisms that drive vascular calcification are manifold and there are several cell types potentially involved. Medial calcification appears to arise mainly from osteogenic transdifferentiation of resident smooth muscle cells [23, 26] or mesenchymal cells, such as adventitial cells and pericytes [12, 20]. On the other hand, circulating calcifying cells may contribute to intimal calcification within atherosclerotic lesions or heart valves, by recruitment from the bone marrow and bloodstream [7, 9, 20]. According to recent data [12], a new paradigm indicates that circulating calcifying cells may have pathophysiological, clinical and therapeutic implications in vascular and bone disorders. We have recently identified a subpopulation of circulating monocyte/macrophage lineage cells which show calcifying ability using in vitro assays and in vivo models of ectopic calcification, such as the subcutaneous Matrigel plug. Such cells express osteocalcin (OC) and bone alkaline phosphatase (BAP), retain myeloid features and are increased in the circulation and bone marrow of diabetic patients [11]. These myeloid calcifying cells (MCCs) can also be obtained after culture of peripheral blood mononuclear cells (PBMCs) and undergo calcification in vitro and when implanted into subcutaneous Matrigel plugs [11]. Although OC^+BAP^+ cells were more frequent in extensively calcified atherosclerotic lesions of diabetic patients compared to less calcified lesions of non diabetic patients, whether MCCs from the bloodstream truly contribute to vascular calcification was unclear. Therefore, the present study was designed to test the hypothesis that OC^+BAP^+ cells promote calcification of atherosclerotic lesions in mice.

MATERIALS AND METHODS

Animals. C57Bl/6 mice constitutively expressing GFP (strain C57BL/6-Tg(CAG-EGFP)1Osb/J from Charles River laboratories) were used as donors of bone marrow cells to be injected into 8- or 40-week old ApoE$^{-/-}$ mice (strain C57Bl/6.129P2-Apoe^{tm1Unc}J from Charles River laboratories). Wild type C57Bl/6 mice were from the in-house colony. Eight week old ApoE$^{-/-}$ mice were fed a standard chow diet, housed in controlled humidity and temperature conditions, with free access to food and water for 24 weeks after cell injection to allow development of atherosclerosis. Forty week old ApoE$^{-/-}$ mice, also fed a standard chow diet, had already developed advanced atherosclerosis, and were maintained for 2 weeks after cell injection. Generation of C57Bl/6 ApoE$^{-/-}$AIF-1^{tg} mice has been described previously [18, 19]. Paraffin-embedded samples from 15 week old ApoE$^{-/-}$AIF-1^{tg} and ApoE$^{-/-}$AIF-1^{wt} mice on a standard chow diet were obtained and analyzed. The protocol was approved by the Animal Ethical Committee of the University of Padova and experiments were conducted according to the NIH principles of laboratory animal care (publication no. 85-23, revised 1985).

Culture of murine calcifying cells. Murine calcifying cells were isolated from the mouse spleen as a large source of mononuclear cells, using a protocol similar to that optimized to yield human MCCs [11]. The spleen was surgically removed from wild type C57Bl/6 mice before killing, minced and filtrated to obtain a single cell suspension. Red blood cells were lysed and mononuclear cells separated using Histopaque 1077 (Sigma-Aldrich). Cells ($3x10^6/cm^2$) were plated in 24-well plates coated with Matrigel (Becton Dickinson) for 3 weeks in complete osteogenic medium (MesenCult^{TM} medium + osteogenic stimuli, Stem Cells Technologies Inc.). The medium was changed first after 1 week and then every 3 days. Two weeks after plating, beta-glycerophosphate (final concentration 3.5 mM) was added to the culture for 1 week to stimulate calcium deposition. At the end of the 3-week culture protocol, wells were stained with Von Kossa and Alizarin red.

Flow cytometry and cell sorting. Spleen-derived mononuclear cells from GFP$^+$ animals were stained with PE-conjugated anti-OC (R&D System) and APC-conjugated anti-BAP (R&D Systems, clone B4-78) monoclonal antibodies for cell sorting (BD FACSAria). GFP$^+$ sorted cells were injected into ApoE$^{-/-}$ mice via the tail vein ($5x10^5$/animal).
For further characterization of spleen-derived OC$^+$BAP$^+$ cells, in separate experiments, cells were co-stained with FITC-conjugated anti-mouse CD45, CD11b, CD3, CD90, CD29, CD44 monoclonal antibodies (all from BD). The percentage of these leukocyte and mesenchymal markers on OC$^+$BAP$^+$ cells was quantified and compared to expression in OC$^-$BAP$^-$ cells on a FACSCanto instrument (BD). AIF-1 detection by FACS was performed on gated human OC$^+$BAP$^+$ and OC$^-$BAP$^-$ cells using a FITC-conjugated clone Iba1 mAb (Abcam cat# AB15691). Flow cytometry was also used to track and characterize GFP$^+$ cells retrieved from peripheral blood, bone marrow and spleen of injected mice, at time of killing. After gating the GFP$^+$ signal, cells were analyzed for the percentage expression of OC and BAP.

In vivo calcification assay. To test the ability of sorted cells to calcify, we performed an in vivo assay by implanting freshly sorted murine OC$^-$BAP$^-$ and OC$^+$BAP$^+$ cells embedded into 500 µL of Matrigel (BD) into the flanks of C57Bl/6 recipient mice. Ten days later, before killing, mice were subjected to a micro computed tomography scan on a microCT eXplore Locus system (GE Healthcare).

Transendothelial migration. To test the ability of OC$^+$BAP$^+$ cells to undergo transendothelial migration, we used a modified transwell migration assay, as previously described [16]. Briefly, freshly isolated, unlabelled PBMC from healthy young blood donors were left to adhere to or transmigrate through a monolayer of green fluorescence-labelled (PKH67, Sigma Aldrich) human aortic endothelial cells (HAECs, Lonza) grown to confluence on the filter membrane of sterile 3 micron-pore, 12-well format transwell migration inserts (BD

Falcon). After 6 hours, transmigrating PBMC were harvested from the lower compartment, while non-adherent (floating) and adherent cells were harvested from the upper compartment by sequential washing/detachment. The 3 cell fractions (floating, adherent and migrated) were individually stained with OC and BAP as described above, to look for enrichment of OC^+BAP^+ cells. Endothelial cells were separated from PBMC during the analysis by a multiparametric gating strategy. Experiments were performed with 3 different PBMC donors each time in duplicate. Higher percentages of OC^+BAP^+ cells in the adhered and migration fraction were considered indicative of selective transendothelial migratory capacity compared with OC or BAP-negative cells.

Culture of VSCM with conditioned media. To test the capacity of circulating calcifying cells to modulate SMC calcification via paracrine signals, bovine aortic smooth muscle cells (BSMCs) were coltured with conditioned media from human OC^+BAP^+ or OC^-BAP^- cells. Explant-derived primary BSMCs were used between passage 4 and 6 and cultured in plastic dishes as previously described [22]. At confluence in 24-well plates, cells were treated with 400 µL of cell culture media (DMEM containing 5% FBS, 100 U/mL penicillin, 100 µg/mL streptomycin) supplemented with 100 µL of 24h-conditioned media from freshly sorted OC^+BAP^+ or OC^-BAP^- cells. To promote calcium deposition, Pi was added to the culture (final concentration 2.0 mmol/L) and the media was changed every third day. After 6 days calcium deposition was quantified by using the O-cresolphtalein complexone method (Chema Diagnostica, Italy). To test the pro-calcific effect of AIF-1, SMC were incubated with 0-1-5 nM recombinant human AIF-1. Experiments were performed in triplicate.

Gene expression analysis. Cells used for these analysis were derived by FACS sorting of OC^-BAP^- and OC^+BAP^+ cells from PBMC obtained by healthy young blood donors.
Microarray. Total RNA was isolated using TRIzol (Invitrogen) followed by cleanup with the RNeasy Mini Kit (Qiagen). RNA integrity was evaluated with the Agilent 2100 Bioanalyzer (Agilent Technologies, Palo Alto, CA) and quantified with a NanoVue spectrophotometer (GE Healthcare Life Sciences, Baie d'Urfe, QC). For gene expression profiling, 250ng of RNA was hybridized to Human Genome U133 Plus 2.0 Arrays (Affymetrix). Expression values were generated from fluorescence signals using the robust multi-array average procedure. Specifically, intensity levels have been background adjusted, normalized using quantile normalization, and log2 expression values calculated using median polish summarization and Entrez custom chip definition files for human arrays (version 15.1.0). The gene expression data are published online at GEO series GSE47060.
Real time quantitative PCR. Total RNA was extracted using RNeasy kit (Qiagen), then reverse transcribed to generate cDNA using the First-Strand cDNA Synthesis Kit from Invitrogen. Gene-specific primer pairs were designed using Primer-BLAST (NCBI) and were validated prior to use by gradient PCR and gel analysis to test for optimal annealing temperature, reaction efficiency and specificity. Real time PCR with Fast SYBR Green detection was performed using an 7900HT Fast Real-Time qPCR System (Applied Biosystems) and the following primers: mouse Ubiquitin C (reference gene) FW 5'GCCCAGTGTTACCACCAAGA 3' RV 5'CCCATCACACCCAAGAACA 3'; mouse AIF-1 FW 5' GTTTGGACGGCAGATCCTCA 3' RV 5' CAGGGATTTGCAGGGAGGAA 3' ; Human Actin beta (reference gene) FW5' GGATGCCACAGGACTCCA 3'; RV5' AGAGCTACGAGCTGCCTGAC 3'; human AIF-1 FW5' ACCAGGGATTTACAGGGAGG 3' RV5' GTTTGGAGGGCAGATCCTCA 3'. GFP-FW 5'CTTCTTCAAGTCCGCCATGC 3' REV 5'GTGTCGCCCTCGAACTTCAC 3'. Expression data were normalized to the mean of housekeeping gene ubiquitin C to control the variability in expression levels and were analyzed using the $2(-\Delta\Delta CT)$ method.

Proteomic analysis. Circulating cells were lysed by sonication on ice in a hypotonic buffer (50 mM HEPES pH 7.5, 1% Triton, protease inhibitor cocktail). Proteins (120 µg) from each sample were precipitated overnight at -20 °C with cold acetone. Protein pellets were dissolved in 120 µl of TEAB 0.5 M, reduced, alkylated and trypsin digested according to the

iTRAQ manufacturer's instructions. Samples were split in two aliquots of 60 µg to perform two technical replicates with tag swapping. Following iTRAQ labelling, samples were pooled and vacuum concentrated. The dried iTRAQ labeled sample was dissolved in 400 µl of equilibration buffer (5 mM KH2PO4, 25% acetonitrile, pH 2.9), and fractionated with a strong cation exchange cartridge (AB Sciex, Canada) in a step-wise mode, using the following concentrations of KCl: 50, 100, 150, 200, 350 mM. Each SCX fraction was then dried under vacuum, resuspended in 500 µl of 0.1% formic acid, desalted using C18 cartridges (Sep-Pack, C18, Waters). Samples from each SCX fraction were dried under vacuum and then dissolved in 50 µl of 0.1% formic acid, obtaining a final concentration of 1 µg/µl. The MS analyses were performed on a LTQ-Orbitrap XL mass spectrometer (Thermo Fisher Scientific) coupled with a nano-HPLC Ultimate 3000 (Dionex - Thermo Fisher Scientific). The same samples fractionated with a Tempo™ LC MALDI Spotting System (AB Sciex) were also analyzed with a MALDI-TOF/TOF 4800 mass spectrometer (AB Sciex). Collected data were analyzed using Proteome Discoverer 1.2 (Thermo Fisher Scientific) connected to a Mascot Search Engine (version 2.2.4, Matrix Science, UK). MS/MS data obtained from from each SCX fraction and with the different instrumental platforms were treated as technical replicate for quantification purposes. Data were filtered considering as positive hits the proteins identified with at least two unique peptides with medium confidence (FDR 5%) and quantified with at least 2 independent peptides. OC^+BAP^+ over OC^-BAP^- cell ratio ≥1.6 was set as threshold for protein over-expression.

Histology and confocal microscopy. $ApoE^{-/-}$ mice injected with $GFP^+OC^+BAP^+$ or $GFP^+OC^-BAP^-$ cells (n=5/group for both long-term and short-term experiments) were killed and dissected under a surgical microscope to collect the aortic sinus, aortic arch, and innominate arteries. Seven-micrometer thick transversal cryosections at each atherosclerotic site were stained with Von Kossa and Alizarin red for analysis of atherosclerotic calcification. The pentachromic staining was used to characterize atherosclerotic lesion components, according to the manufacturer's instructions (American MasterTech). Custom ImageJ plug-ins were used for quantification of calcium deposits.
For extraction and quantification of calcium from paraffin-embedded tissue samples of 15 week old AIF-1Tg $ApoE^{-/-}$ and control mice, paraffin was removed by melting blocks at 60°C. Tissues samples were put in xylene 100% for 10 minutes at room temperature and then Hydrated through a descending alcohol series to water. Samples were put in 100 ul HCl 0.6 N, heated at 99° for 5 minutes and lysed through 2 cycles of freezing and thawing by snap freezing in liquid nitrogen and thawing on ice. Samples were left overnight in HCl 0.6 N before mechanical disruption with TissueLyser (Qiagen). HCl was neutralised with 100 ul of 0.1 N NaOH, 0.1% SDS. Samples were centrifuged at room temperature at 13000xG. Surnatant were assed for calcium concentration by using O-cresolphtalerin complexome method (Chema Diagnostica, Italy). Protein concentration was assessed by using NanoVue Plus (Ge Life Sciences).
To track the fate of injected GFP^+ cells, we tried different strategies of confocal microscopy (Leica TCS SP5). The endogenous GFP signal was weak and barely above background green signal, determined by necrotic debris, oxidized lipids and calcium deposits within atherosclerotic lesions. When stained with an anti-GFP antibody (Rabbit Anti-GFP, Life Technologies, UK) and green secondary antibody (Donkey Anti-Rabbit DyLight 488, Jackson ImmunoResearch, UK), signal amplification was insufficient to discriminate positive areas from the background. We therefore used a blue-labelled secondary antibody (Donkey Anti-Rabbit AMCA, Jackson) to amplify the GFP signal and nuclei were counterstained in red with propidium iodine (PI). With this combination, only cells with simultaneous blue and green cytoplasm and a defined red nuclear shadow were considered as homed GFP^+ cells.

Statistical analysis. Data are expressed as mean ± standard error. Comparison between 2 or more groups were performed using ANOVA and Student's t test, respectively. Bonferroni correction was applied to account for multiple testing and statistical significance was accepted at $p<0.05$.

RESULTS

Isolation of murine calcifying cells. We have previously shown that culture of human PBMC in osteogenic conditions yields a population of OC- and BAP- expressing cells that calcify in vitro and in vivo. Herein, we have used a similar protocol to isolate murine calcifying cells in vitro: spleen-derived mononuclear cells were able to mineralize 3 weeks after plating, as shown by Von Kossa and Alizarin red staining (Figure 1). These data suggest that the spleen harbours a subset of calcifying cells, that can be used for in vivo experiments.

Murine OC^+BAP^+ cells promote ectopic calcification in vivo. Using FACS, we isolated OC^+BAP^+ and OC^-BAP^- cells from the spleen of C57Bl/6 mice to obtain a pure population of calcifying cells and the respective control cells. By surface immunophenotyping, we found that OC^+BAP^+ cells expressed leukocyte (CD45) and myeloid (CD11b, CD29, CD44) markers with no expression of the mesenchymal stem cell marker CD90 (Thy-1). Importantly, compared to OC^-BAP^- cells, OC^+BAP^+ cells expressed higher levels of the adhesion molecules CD11b and CD29, which are important for homing to the vascular wall. Freshly sorted murine OC^+BAP^+ and OC^-BAP^- cells were embedded into Matrigel plugs and implanted subcutaneously into the flanks of syngeneic C57Bl/6 mice. After 2 weeks, mice were subjected to a MicroCT scan, that revealed the presence of grossly calcified nodules at the sites of OC^+BAP^+ cell implantation, while no calcification was seen by contralateral OC^-BAP^- cells (Figure 1).

OC^+BAP^+ cells undergo transendothelial migration in vitro. We reasoned that the capacity of circulating calcifying cells to promote atherosclerotic calcification might be linked to their transendothelial migration activity. We tested the ability of human OC^+BAP^+ cells to adhere and transmigrate across an endothelial layer using a modified transwell assay with human aortic endothelial cells (HAEC). We found that the percentage of OC^+BAP^+ cells in the adherent and migrated fraction was significantly enriched than in the floating compartment, indicating the selective adherence and transendothelial migration of OC^+BAP^+ cells compared to OC- or BAP-negative cells (Figure 2).

Murine OC^+BAP^+ cells promote calcification of early and advanced atherosclerosis. To test the hypothesis that OC^+BAP^+ cells promote atherosclerotic calcification, we injected these cells into $ApoE^{-/-}$ mice using either a long term experiment in young mice (EXP-1) or a short-term experiment in aged mice (EXP-2). Figure 3A shows the experimental design.
Freshly isolated OC^+BAP^+ or OC^-BAP^- cells (5×10^5 / mouse) from the spleen of mice constitutively expressing GFP were injected into 8-wks old $ApoE^{-/-}$ mice, fed a standard chow diet for 24 weeks. Before euthanasia, blood, spleen and bone marrow cells were collected for FACS analysis. After 24 weeks, GFP^+ cells were still present in the bloodstream and accounted for about 0.01% of circulating leukocytes. OC^+BAP^+ cells were preferentially found in peripheral blood, while OC^-BAP^- cells were preferentially located in the bone marrow. For both OC^+BAP^+ and OC^-BAP^- cells, about 60% of injected GFP^+ cells that were still present in the circulation retained their original phenotype, while the remaining 40% had lost or acquired OC and/or BAP (Figure 3).
Atherosclerotic lesions in young $ApoE^{-/-}$ mice fed a standard chow diet for 24 weeks were mainly located in the aortic sinus. Von Kossa and Alizarin red staining showed a 2.3-fold higher degree of calcification (% calcified area) in mice injected with OC^+BAP^+ compared to mice injected with control OC^-BAP^- cells (Figure 4A). Freshly isolated OC^+BAP^+ or OC^-BAP^- GFP^+ cells were also injected into 40-wks old $ApoE^{-/-}$ mice, fed a standard chow diet for 2 weeks. Two weeks after injection, GFP^+ cells were present in the bloodstream and accounted for about 0.01% of circulating leukocytes. These mice had developed extensive atherosclerotic lesions. Mice injected with OC^+BAP^+ cells showed increased calcified areas in the innominate artery, aortic arch and aortic sinus compared to mice injected with OC^-BAP^- cells and to non-injected coeval $ApoE^{-/-}$ mice, used as controls (Figure 4B).

Characterization of lesion components was performed with pentachrome (Movat's) staining, in which black colouring is for nuclei and elastic fibres, yellow for collagen fibres, blue for mucin and bright red for fibrin and red for muscle. Lesions derived from old ApoE$^{-/-}$ mice (EXP-2) injected with OC^{+}BAP^{+} cells showed significant changes in such components. Compared to injection of OC^{-}BAP^{-} cells, injection of OC^{+}BAP^{+} cells increased collagen accumulation in the innominate artery and aortic arch and increased mucin content in the aortic arch and sinus, while other components showed no changes (Figure 5).

Presence of injected cells at sites of vascular disease. In order to track the fate of injected cells, we used different strategies to detect the GFP signal. Several apparently spontaneously green fluorescent cells (nuclei surrounded by green fluorescence, Figure 6A) were detectable in sections of atherosclerotic lesions, but non-specific signal was also abundant and the hypothetical GFP signal was barely above the background, especially near areas of oxidized lipid accumulation and calcification. Amplification of the GFP signal with an indirect green fluorescent immunodetection slightly improved resolution, but did not allow a clear discrimination from background, especially in advanced and complex lesions. Therefore, we used a blue-conjugated indirect anti-GFP staining and counterstained nuclei in red because autofluorescence of atherosclerotic lesions was lower in the blue than in the green channel. This allowed us to better identify injected cells as a red nucleus surrounded by a blue cytoplasm (anti-GFP) co-localized with endogenous green fluorescence (Figure 6B-D). With this specific method, we detected a very small number of injected cells within atherosclerotic lesions (on average less than 1 cell per section), with no difference in atherosclerotic areas of mice injected with OC^{+}BAP^{+} compared to mice injected with OC^{-}BAP^{-} cells. As this highly specific method may lead to an underestimation of the amount of GFP^{+} cells in the lesions, we performed a qPCR analysis of the GFP mRNA in vascular specimen extracts obtained from OC^{+}BAP^{+} and OC^{-}BAP^{-} cell-injected mice of both EXP-1 and EXP-2. We found that the GFP transcript was undetectable (or below detection limit) at both timepoints, as it was undistinguishable from the negative control represented by a non-GFP tissue (Figure 6E). Sequencing of the late amplification products revealed only no GFP signal (not shown). These data indicate that the local contribution of injected MCCs to atherosclerotic calcification is very small or negligible and we hypothesize that they may affect calcification of resident cells by paracrine signals.

Allograft inflammatory factor-1 contributes to the paracrine pro-calcific activity of MCCs. To dissect the molecular mechanisms driving the pro-calcific potential of MCCs, we performed an extensive genomic and proteomic investigation of human OC^{+}BAP^{+} cells (MCCs) relative to control OC^{-}BAP^{-} cells. We aligned gene and protein IDs to identify those that were significantly upregulated in MCCs and found 57 genes/proteins (Online Resource 1, Figure 7A). A pathway analysis run on the DAVID platform [15] identified calcium handling as the second most enriched functional annotation cluster. Among calcium-binding proteins, allograft inflammatory factor-1 (AIF-1) was strongly upregulated as gene (4.6-fold) and protein (3.1-fold). We validated AIF-1 mRNA upregulation in freshly sorted human and mouse OC^{+}BAP^{+} versus OC^{-}BAP^{-} cells, as well as AIF-1 protein expression by flow cytometry on human cells (Figure 7B). Based on the paracrine hypothesis, VSMC were challenged with conditioned media from freshly isolated human OC^{+}BAP^{+} cells or control OC^{-}BAP^{-} cells. We found that VSMC exposed to OC^{+}BAP^{+} cell conditioned medium showed a 2.5-fold higher calcification compared to the control medium and a significant 40% increased calcification compared to VSMC exposed to OC^{-}BAP^{-} cell conditioned medium. In addition, VSMC incubated with 5 nM AIF-1 showed increased calcification compared with the control condition (Figure 7C).

To confirm that excess AIF-1 expression drives vascular calcification by MCCs in vivo, we analyzed samples from ApoE$^{-/-}$AIF-1^{tg} mice, in which overexpression of AIF-1 is driven by the CD11b promoter and is thus specific for the monocyte-macrophage lineage, to which MCCs belong. It has been shown previously that these mice have accelerated atherosclerosis [18]. After calcium extraction from tissue samples including the aortic sinus, aortic valve and aortic

arch, we found that, compared to control ApoE$^{-/-}$ mice, ApoE$^{-/-}$AIF-1^{tg} mice have a marked increase in calcium content (Figure 7D).

DISCUSSION

We show that injection of OC^+BAP^+ cells into young and old $ApoE^{-/-}$ mice strongly increased calcification of early and advanced atherosclerotic lesions. We have recently demonstrated that human OC^+BAP^+ cells derive from the myeloid lineage, form mineralized nodules in vitro and calcify when implanted subcutaneously into nude mice. These myeloid calcifying cells (MCCs) were detected by immunohistochemistry in atherosclerotic lesions and their circulating levels were increased in patients with diabetes and/or cardiovascular disease, but it was unclear whether circulating OC^+BAP^+ cells homed to the diseased vessel wall or they contributed to calcification through other mechanisms. Herein, we first show that OC^+BAP^+ cells have a selective capacity to adhere and migrate across the endothelium, lending support to their involvement in vascular disease. Second, we found that the murine spleen contains a subpopulation of mononuclear cells that calcify in vitro. Spleen-derived OC^+BAP^+ cells calcified in vivo and displayed an antigenic profile similar to that of human MCCs. OC^+BAP^+ cells had a higher expression of integrin adhesion molecules CD11b and CD29 than control OC^-BAP^- cells, again supporting their vasculotrophic activity. Therefore, we devised a cell transfer protocol to study the ability of labelled OC^+BAP^+ MCCs and control OC^-BAP^- cells to modulate calcification in the atherosclerosis-prone $ApoE^{-/-}$ mice, as a proof-of-concept of the MCC activity in vivo. We studied both early and advanced lesions 24 and 2 weeks after cell injection, respectively. Remarkably, 60% of injected GFP^+ cells maintained their original phenotype (OC^+BAP^+ or OC^-BAP^-) and represented 0.01% of circulating leukocytes at 24 weeks after injection. This indicates that injected cells steadily circulated in the recipient mice. While injected OC^+BAP^+ cells were present mainly in the bloodstream and not in the bone marrow, OC^-BAP^- cells repopulated the bone marrow to a small extent. These findings are in line with the previous observations that human OC^+BAP^+ cells, unlike OC^-BAP^- cells, are long lived and not necessarily residing in the bone marrow [11]. We used the spleen as a source of cells to be injected into $ApoE^{-/-}$ mice because it has been recently shown that the spleen functions as a buffer of monocytic cells that accelerate atherosclerosis [8], and is a candidate reservoir of MCCs. In addition, OC^+BAP^+ cells from the bone marrow would be contaminated by mesenchymal stem cells expressing OC and BAP [21], which are rarer in the spleen.

The most striking result of the present study is that injection of OC^+BAP^+ cells into $ApoE^{-/-}$ mice strongly increased atherosclerotic calcification of early lesions over 24 weeks and of advanced lesions over 2 weeks. This is the sought proof-of-concept demonstration that MCCs are involved in atherosclerotic calcification in vivo and supports the role of circulating cells in this phenomenon [12]. To track the fate of injected cells, we used a genetic approach in which cells are spontaneously fluorescent owing to genomic expression of GFP. Detection of GFP signal in atherosclerotic areas is complicated by the extensive autofluorescence of necrotic debris, oxidized lipids and calcium deposits. It has been demonstrated that a multiparametric and stringent confocal microscopy analysis is needed to reliably detect the presence of injected in cardiovascular tissues [4, 5]. Thus, the simple enumeration of green fluorescent cells in the sections of complex tissues likely leads to an overestimation of the homing phenomenon. To overcome this bias, we used specific and stringent criteria to detect injected cells and found that, despite the strong effect on calcification, the number of injected cells present in the lesions at time of sacrifice was very low. Consistently, qPCR performed on RNA isolated from atherosclerotic lesions of mice injected with GFP^+ OC^+BAP^+ and OC^-BAP^- cells was unable to detect the GFP transcript. The most reasonable explanation are that either OC^+BAP^+ die in the process of calcification or that calcification results from a paracrine activity. As it would be surprising that extensive neointimal calcifications were entirely attributable to circulating cells, we hypothesized that OC^+BAP^+ cells might indirectly promote calcification of smooth muscle cells, the most abundant source of calcifying cells in the vessel wall [27]. Indeed, conditioned medium obtained from OC^+BAP^+ cells induced calcification of VSMC more than conditioned medium from OC^-BAP^- cells. To dissect the molecular machinery driving the pro-calcific potential of MCCs, we performed an in-depth and unprecedented genomic and proteomic investigation. We detected a series of 57 genes

and their products that were upregulated in OC^+BAP^+ cells compared to OC^-BAP^- controls. Much interestingly, the calcium handling functional annotation pathway, which is involved in calcification, was enriched in this cluster of genes/proteins. Indeed, 12/57 genes/proteins (21%) have calcium-binding activity and AIF-1 was among the most upregulated ones. AIF-1 has been previously shown to induce atherosclerosis, restenosis and vascular inflammation by stimulation of VSMC and monocyte-macrophage activity [3, 18, 24, 29]. SM-restricted AIF-1 overexpressing mice on a high fat diet develop accelerated atherosclerosis [24]. By converse, in vivo AIF-1 silencing decreased neointimal hyperplasia in wire-injured rat carotid arteries [25]. AIF-1 is induced by interferon-γ, which affects the VSMC phenotype [6]. Therefore, we focused on AIF-1 as a candidate mediator of the pro-calcific potential of MCCs. AIF-1 was able to induce calcification of cultured VSMC, supporting the paracrine hypothesis. Furthermore, transgenic $ApoE^{-/-}$ mice with CD11b-driven AIF-1 overexpression showed exacerbated aortic calcification, strongly indicating that AIF-1 activity in monocyte-macrophages stimulates vascular calcification and further supporting the role of AIF-1 in MCCs. Despite atherosclerosis in these 15-weeks old AIF-1^{tg} mice fed a chow diet was mainly located at the aortic sinus, detailed information about the exact site of excess calcification (plaques, valves, whole aorta, media or adventitia) is presently missing and is a matter of future research. AIF-1 is an actin-binding protein that is also secreted in the extracellular fluids and its serum concentrations are correlated with cardiovascular risk factors [14]. This notion supports the potential role of AIF-1 as a MCC-derived systemic paracrine factor.

In addition to AIF-1, several other calcium-binding proteins were found to be upregulated in MCCs, including S100-A8/9 that have been previously implicated in atherosclerosis [1]. Therefore, mechanisms other than AIF-1 likely contribute to the pro-calcific effect of MCCs, explaining why AIF-1 supplementation induced a smaller increase in VSMC calcification compared to MCC conditioned medium.

The paracrine hypothesis reconciles the low number of GFP^+ cells in the lesions with the extensive calcifications and also provides an explanation for the inconsistent literature about the role of circulating cells in vascular calcification [12]. Using genetic lineage tracking models, Naik et al. recently reported that most (80-98%) calcifying cells in atherosclerotic lesions of $ApoE^{-/-}$ and $LDLr^{-/-}$ mice are derived form local smooth muscle cells and that circulating cells provide a much smaller contribution [20]. Herein, we suggest that the paracrine activity of circulating myeloid cells is critical for stimulation of calcification by resident cells. This scenario is not surprising, as myeloid cells play major roles in the development and progression of atherosclerosis, mainly by secretory activity and release of cellular components upon cell death [13, 17, 28, 30]. In addition, this figure is similar to that shown for BM-derived smooth muscle cells, which are rarely found in atherosclerotic plaques, but significantly promote development of the lesion [31]. In this framework, our data indicate that OC^+BAP^+ cells are the pro-calcific subpopulation of monocytes, and suggest these MCCs and AIF-1 represent therapeutic targets to counter vascular calcification.

Acknowledgements: none.

Sources of funding: GPF is supported by a European Foundation for the Study of Diabetes (EFSD) / AstraZeneca young investigator award.

Conflict of interest: none.

Disclosures: none.

REFERENCES

1. Averill MM, Kerkhoff C, Bornfeldt KE (2012) S100A8 and S100A9 in cardiovascular biology and disease. Arterioscler Thromb Vasc Biol 32:223-229. doi:10.1161/ATVBAHA.111.236927
2. Baars T, Kleinbongard P, Bose D, Konorza T, Mohlenkamp S, Hippler J, Erbel R, Heusch G (2012) Saphenous vein aorto-coronary graft atherosclerosis in patients with chronic kidney disease: more plaque calcification and necrosis, but less vasoconstrictor potential. Basic Res Cardiol 107:303. doi:10.1007/s00395-012-0303-3
3. Berglund LM, Kotova O, Osmark P, Grufman H, Xing C, Lydrup ML, Goncalves I, Autieri MV, Gomez MF (2012) NFAT regulates the expression of AIF-1 and IRT-1: yin and yang splice variants of neointima formation and atherosclerosis. Cardiovasc Res 93:414-423. doi:10.1093/cvr/cvr309
4. Cevese A (2012) Totipotent stem cells could do everything ... or else nothing: the case of vascular reendothelialization. Cardiovasc Res 93:211-212. doi: 10.1093/cvr/cvr342.
5. Deb A, Patterson C (2010) Hard luck stories: the reality of endothelial progenitor cells continues to fall short of the promise. Circulation 121:850-852. doi:CIR.0b013e3181d4c360
6. Demyanets S, Kaun C, Rychli K, Pfaffenberger S, Kastl SP, Hohensinner PJ, Rega G, Katsaros KM, Afonyushkin T, Bochkov VN, Paireder M, Huk I, Maurer G, Huber K, Wojta J (2011) Oncostatin M-enhanced vascular endothelial growth factor expression in human vascular smooth muscle cells involves PI3K-, p38 MAPK-, Erk1/2- and STAT1/STAT3-dependent pathways and is attenuated by interferon-gamma. Basic Res Cardiol 106:217-231. doi:10.1007/s00395-010-0141-0
7. Doehring LC, Heeger C, Aherrahrou Z, Kaczmarek PM, Erdmann J, Schunkert H, Ehlers EM (2010) Myeloid CD34+CD13+ precursor cells transdifferentiate into chondrocyte-like cells in atherosclerotic intimal calcification. Am J Pathol 177:473-480. doi: 10.2353/ajpath.2010.090758
8. Dutta P, Courties G, Wei Y, Leuschner F, Gorbatov R, Robbins CS, Iwamoto Y, Thompson B, Carlson AL, Heidt T, Majmudar MD, Lasitschka F, Etzrodt M, Waterman P, Waring MT, Chicoine AT, van der Laan AM, Niessen HW, Piek JJ, Rubin BB, Butany J, Stone JR, Katus HA, Murphy SA, Morrow DA, Sabatine MS, Vinegoni C, Moskowitz MA, Pittet MJ, Libby P, Lin CP, Swirski FK, Weissleder R, Nahrendorf M (2012) Myocardial infarction accelerates atherosclerosis. Nature 487:325-329. doi: 10.1038/nature11260
9. Egan KP, Kim JH, Mohler ER, 3rd, Pignolo RJ (2011) Role for circulating osteogenic precursor cells in aortic valvular disease. Arterioscler Thromb Vasc Biol 31:2965-2971. doi:ATVBAHA.111.234724
10. Erbel C, Dengler TJ, Wangler S, Lasitschka F, Bea F, Wambsganss N, Hakimi M, Bockler D, Katus HA, Gleissner CA (2011) Expression of IL-17A in human atherosclerotic lesions is associated with increased inflammation and plaque vulnerability. Basic Res Cardiol 106:125-134. doi:10.1007/s00395-010-0135-y
11. Fadini GP, Albiero M, Menegazzo L, Boscaro E, Vigili de Kreutzenberg S, Agostini C, Cabrelle A, Binotto G, Rattazzi M, Bertacco E, Bertorelle R, Biasini L, Mion M, Plebani M, Ceolotto G, Angelini A, Castellani C, Menegolo M, Grego F, Dimmeler S, Seeger F, Zeiher A, Tiengo A, Avogaro A (2011) Widespread increase in myeloid calcifying cells contributes to ectopic vascular calcification in type 2 diabetes. Circ Res 108:1112-1121. doi:CIRCRESAHA.110.234088
12. Fadini GP, Rattazzi M, Matsumoto T, Asahara T, Khosla S (2012) Emerging role of circulating calcifying cells in the bone-vascular axis. Circulation 125:2772-2781. doi:125/22/2772
13. Frostegard J, Ulfgren AK, Nyberg P, Hedin U, Swedenborg J, Andersson U, Hansson GK (1999) Cytokine expression in advanced human atherosclerotic plaques:

dominance of pro-inflammatory (Th1) and macrophage-stimulating cytokines. Atherosclerosis 145:33-43. doi:S0021-9150(99)00011-8

14. Fukui M, Tanaka M, Toda H, Asano M, Yamazaki M, Hasegawa G, Imai S, Fujinami A, Ohta M, Nakamura N (2012) The serum concentration of allograft inflammatory factor-1 is correlated with metabolic parameters in healthy subjects. Metabolism 61:1021-1025. doi:10.1016/j.metabol.2011.12.001
15. Huang da W, Sherman BT, Lempicki RA (2009) Systematic and integrative analysis of large gene lists using DAVID bioinformatics resources. Nat Protoc 4:44-57. doi:10.1038/nprot.2008.211
16. Krankel N, Kuschnerus K, Madeddu P, Luscher TF, Landmesser U (2011) A novel flow cytometry-based assay to study leukocyte-endothelial cell interactions in vitro. Cytometry A 79:256-262. doi:10.1002/cyto.a.21043
17. Martinet W, Schrijvers DM, De Meyer GR (2012) Molecular and cellular mechanisms of macrophage survival in atherosclerosis. Basic Res Cardiol 107:297. doi:10.1007/s00395-012-0297-x
18. Mishima T, Iwabuchi K, Fujii S, Tanaka SY, Ogura H, Watano-Miyata K, Ishimori N, Andoh Y, Nakai Y, Iwabuchi C, Ato M, Kitabatake A, Tsutsui H, Onoe K (2008) Allograft inflammatory factor-1 augments macrophage phagocytotic activity and accelerates the progression of atherosclerosis in ApoE-/- mice. Int J Mol Med 21:181-187.
19. Morohashi T, Iwabuchi K, Watano K, Dashtsoodol N, Mishima T, Nakai Y, Shimada S, Nishida R, Fujii S, Onoe K (2003) Allograft inflammatory factor-1 regulates trinitrobenzene sulphonic acid-induced colitis. Immunology 110:112-119. doi: 10.1046/j.1365-2567.2003.01714.
20. Naik V, Leaf EM, Hu JH, Yang HY, Nguyen NB, Giachelli CM, Speer MY (2012) Sources of cells that contribute to atherosclerotic intimal calcification: an in vivo genetic fate mapping study. Cardiovasc Res 94:545-54. doi: 10.1093/cvr/cvs126
21. Post S, Abdallah BM, Bentzon JF, Kassem M (2008) Demonstration of the presence of independent pre-osteoblastic and pre-adipocytic cell populations in bone marrow-derived mesenchymal stem cells. Bone 43:32-39. doi:S8756-3282(08)00140-3
22. Preusch MR, Rattazzi M, Albrecht C, Merle U, Tuckermann J, Schutz G, Blessing E, Zoppellaro G, Pauletto P, Krempien R, Rosenfeld ME, Katus HA, Bea F (2008) Critical role of macrophages in glucocorticoid driven vascular calcification in a mouse-model of atherosclerosis. Arterioscler Thromb Vasc Biol 28:2158-2164. doi:ATVBAHA.108.174128
23. Rattazzi M, Bennett BJ, Bea F, Kirk EA, Ricks JL, Speer M, Schwartz SM, Giachelli CM, Rosenfeld ME (2005) Calcification of advanced atherosclerotic lesions in the innominate arteries of ApoE-deficient mice: potential role of chondrocyte-like cells. Arterioscler Thromb Vasc Biol 25:1420-1425. doi: 10.1161/ 01.ATV.0000166600.58468.1b
24. Sommerville LJ, Kelemen SE, Ellison SP, England RN, Autieri MV (2012) Increased atherosclerosis and vascular smooth muscle cell activation in AIF-1 transgenic mice fed a high-fat diet. Atherosclerosis 220:45-52. doi:10.1016/j.atherosclerosis.2011.07.095
25. Sommerville LJ, Xing C, Kelemen SE, Eguchi S, Autieri MV (2009) Inhibition of allograft inflammatory factor-1 expression reduces development of neointimal hyperplasia and p38 kinase activity. Cardiovasc Res 81:206-215. doi:10.1093/cvr/cvn242
26. Speer MY, Yang HY, Brabb T, Leaf E, Look A, Lin WL, Frutkin A, Dichek D, Giachelli CM (2009) Smooth muscle cells give rise to osteochondrogenic precursors and chondrocytes in calcifying arteries. Circ Res 104:733-741. doi: 10.1161/CIRCRESAHA.108.183053
27. Steitz SA, Speer MY, Curinga G, Yang HY, Haynes P, Aebersold R, Schinke T, Karsenty G, Giachelli CM (2001) Smooth muscle cell phenotypic transition associated

with calcification: upregulation of Cbfa1 and downregulation of smooth muscle lineage markers. Circ Res 89:1147-1154. doi: 10.1161/hh2401.101070

28. Thorp E, Tabas I (2009) Mechanisms and consequences of efferocytosis in advanced atherosclerosis. J Leukoc Biol 86:1089-1095. doi:jlb.0209115
29. Tian Y, Kelemen SE, Autieri MV (2006) Inhibition of AIF-1 expression by constitutive siRNA expression reduces macrophage migration, proliferation, and signal transduction initiated by atherogenic stimuli. Am J Physiol Cell Physiol 290:C1083-1091. doi:00381.2005
30. Vasudevan SS, Lopes NH, Seshiah PN, Wang T, Marsh CB, Kereiakes DJ, Dong C, Goldschmidt-Clermont PJ (2003) Mac-1 and Fas activities are concurrently required for execution of smooth muscle cell death by M-CSF-stimulated macrophages. Cardiovasc Res 59:723-733. doi:S0008636303005145
31. Yu H, Stoneman V, Clarke M, Figg N, Xin HB, Kotlikoff M, Littlewood T, Bennett M (2011) Bone marrow-derived smooth muscle-like cells are infrequent in advanced primary atherosclerotic plaques but promote atherosclerosis. Arterioscler Thromb Vasc Biol 31:1291-1299. doi:ATVBAHA.110.218578

FIGURE LEGENDS

Figure 1. Isolation and characterization of murine MCCs. C57Bl/6 mice were used as donors and cells were isolated from the spleen. Total spleen mononuclear cells were plated in osteogenic medium and showed the presence of calcifying cells. Murine OC^+BAP^+ and OC^-BAP^- cells were isolated by FACS from the spleen mononuclear cell population, embedded in Matrigel plugs and implanted subcutaneously in syngeneic recipient mice. Ten days later, a microCT scan revealed calcifications at sites of OC^+BAP^+ cell implantation. Cells isolated from the murine spleen were also characterized by flow cytometry to determine surface markers expressed by OC^+BAP^+ and OC^-BAP^- cells (*$p<0.05$ versus OC^-BAP^- cells).

Figure 2. Transendothelial migration. A) A modified transwell assay was used to study migration of human mononuclear cells across an endothelial monolayer. B) The floating, adherent and migrated fraction were collected and stained with OC and BAP to identify the 2 cell populations of interest (OC^+BAP^+ and OC^-BAP^-). C) The percentage of OC^+BAP^+, OC^+BAP^-, OC^-BAP^+ and OC^-BAP^- cells in the adhered and migrated fractions are reported as x-fold versus the percentage in the floating fraction. Only OC^+BAP^+ showed significant enrichment in the adhered and migrated fractions, while the other population remained unchanged or showed depletion (*$p<0.05$ versus floating; $^{\#}p<0.05$ versus migrated). On the bottom right, the absolute percentages of the 4 populations of cells in the original PBMC fraction is reported.

Figure 3. Cell injection protocols. A) Design of the cell transfer experiments. We tested whether injection of isolated OC^+BAP^+ MCCs or control OC^-BAP^- cells modified atherosclerotic calcification in recipient $ApoE^{-/-}$ mice. To this end, we devised a long-term (24 weeks) study on young (8-week old) $ApoE^{-/-}$ mice (EXP-1) and a short-term (2 weeks) study on old (40-week) $ApoE^{-/-}$ mice (EXP-2). These complementary experiments provided information on the role of MCCs on calcification of early and advanced atherosclerotic lesions. B-E) Tracking of GFP^+ cells 24 weeks after injection. In EXP-1, 24 weeks after injection, GFP^+ cells accounted for about 0.01% of circulating leukocytes. $GFP^+OC^+BAP^+$ cells (representative plot in B) were about 70% more frequent than $GFP^+OC^-BAP^-$ cells (representative plot in C). $GFP^+OC^-BAP^-$ cells were preferentially located in the bone marrow (D). Interestingly, about 60% of injected $GFP^+OC^+BAP^+$ cells and $GFP^+OC^-BAP^-$ cells maintained their OC and BAP expression profiles 24 weeks after injection (E).

Figure 4. Atherosclerotic calcification. A) In young $ApoE^{-/-}$ mice of EXP-1, atherosclerosis was almost exclusively detected in the aortic sinus. At this site, mice injected with OC^+BAP^+ cells showed more than doubled calcifications compared to mice injected with OC^-BAP^- cells, as assessed by Von Kossa staining (*$p<0.05$; n=5/group). B) In old ApoE-/- mice, atherosclerosis developed extensively in the aortic sinus, innominate artery and aortic arch. At each of these sites, mice injected with OC^+BAP^+ cells showed larger calcified areas compared to mice injected with OC^-BAP^- cells and to non-injected coeval $ApoE^{-/-}$ mice, as assessed by Von Kossa and Alizarin red stainings (*$p<0.05$ versus both OC^-BAP^- and non injected) n=5/group).

Figure 5. Characterization of atherosclerotic lesions. Sections from atherosclerotic lesions of OC^+BAP^+ and OC^-BAP^- cell injected mice were stained using the pentachrome protocol in which the black colouring is for nuclei and elastic fibres, yellow for collagen fibres, blue for mucin and bright red for fibrin and red for muscle. Representative sections are shown. Quantification was performed for collagen and mucin content and for other components (elastic fibers, muscle and fibrin) altogether (*$p<0.05$ for OC^+BAP^+ versus OC^-BAP^-).

Figure 6. Tracking of injected cells in atherosclerotic lesions. For tracking injected GFP^+ cells in atherosclerotic areas, we used different strategies (see text). Representative confocal

microscopy images show nuclei in red, anti-GFP immunostaining in blue, and spontaneous GFP signal in green. A) Several putative GFP+ injected cells in a section of atherosclerotic plaque from mice injected with OC+BAP+ cells in EXP-2 (arrowheads). B) Two putative GFP^+ cells within an innominate atherosclerotic lesion of a mice injected with OC^+BAP^+ cells in EXP-2. Inserts in the upper lane show a nucleated (red) cell with a green and blue GFP^+ cytoplasm (arrow), interpreted as an injected cell. Within a few micrometers, an unspecific GFP signal in present (asterisk). Inserts in the bottom lane show a calcified area that was hyperfluorescent in all channels, suggesting an unspecific signal. However, the central nuclear shadow in the green and blue channel might indicate the presence of a calcified injected cell. C) A putative injected GFP+ cells close to a small calcification within an aortic arch atherosclerotic lesion of a mice injected with OC^+BAP^+ cells in EXP-2. Inserts show a red nucleus surrounded by blue and green GFP+ cytoplasm (arrow). In the close vicinity, an enlongated vertical calcification, hyperfluorescent in all channels and devoid of a nuclear shadow (asterisk) can be interpreted as a calcification. D) A nucleated cells with cytoplasmic GFP signal in the green and blue channel close to a non-GFP cell and a non-nucleated green and blue signal. Scale bar 50 micron. E) qPCR analysis of the GFP transcript in RNA samples extracted from atherosclerotic specimen of OC^+BAP^+ or OC^-BAP^- cell injected mice (samples of interest). The positive and controls were muscle samples from a constitutively expressing GFP mouse and a wild type (GFP-neg) mouse, respectively. The amplification plots show that there was no difference between the samples of interest and the negative control. Sequencing of the amplification products from the samples of interest revealed no GFP sequence.

Figure 7. Transcriptomic/proteomic analysis of MCCs and AIF-1 validation. A) The discovery strategy to detect gene/proteins potentially associated with calcification. Fold-change enrichment values in human OC^+BAP^+ versus OC^-BAP^- cells for gene and protein expression and reported in the scatter plot. We selected the most upregulated gene/proteins based on the arbitrary 1.6-fold enrichement threshold. Alignment of these 57 genes with the respective proteins is reported in Online Table 1. A pathway analysis run on the David platform identified 7 pathways with the reported enrichment score. Based on functional annotation of this sample of gene/proteins, we extracted calcium-binding proteins, as those potentially involved in ectopic calcification. Their protein and gene enrichment in OC^+BAP^+ versus OC^-BAP^- cells is reported. B) Overexpression of AIF-1 on OC^+BAP^+ versus OC^-BAP^- cells was validated by gene expression in sorted mouse and human cells, and was also confirmed by flow cytometry identification of the protein in human gated OC^+BAP^+ and OC^-BAP^- cells. C) Bovine VSMC cells were cultured for 6 days in the presence of control medium (CTRL) or conditioned medium from human OC^-BAP^- and OC^+BAP^+ cells (left panel), or with increasing concentrations of AIF-1 (right panel). Each condition was supplemented with inorganic phosphate to obtain a final concentration of 2.0 mmol/L. Calcification was estimated by quantifying the calcium/protein ratio at the end of the culture period. *$p<0.05$ compared to control (n=3/condition). D) The role of AIF-1 overexpression in vascular calcification was validated in vivo by analyzing the extent of calcium content in tissue samples including the aortic sinus, valves and arch of myeloid specific (CD11b-driven) overexpressing (TG) $ApoE^{-/-}$ mice and the relevant $ApoE^{-/-}$ controls (*$p<0.05$). The left panel shows representative histological staining of the aortic sinus showing increased atherosclerosis in ApoE-/- $AIF\text{-}1^{TG}$ mice.

Figure 1

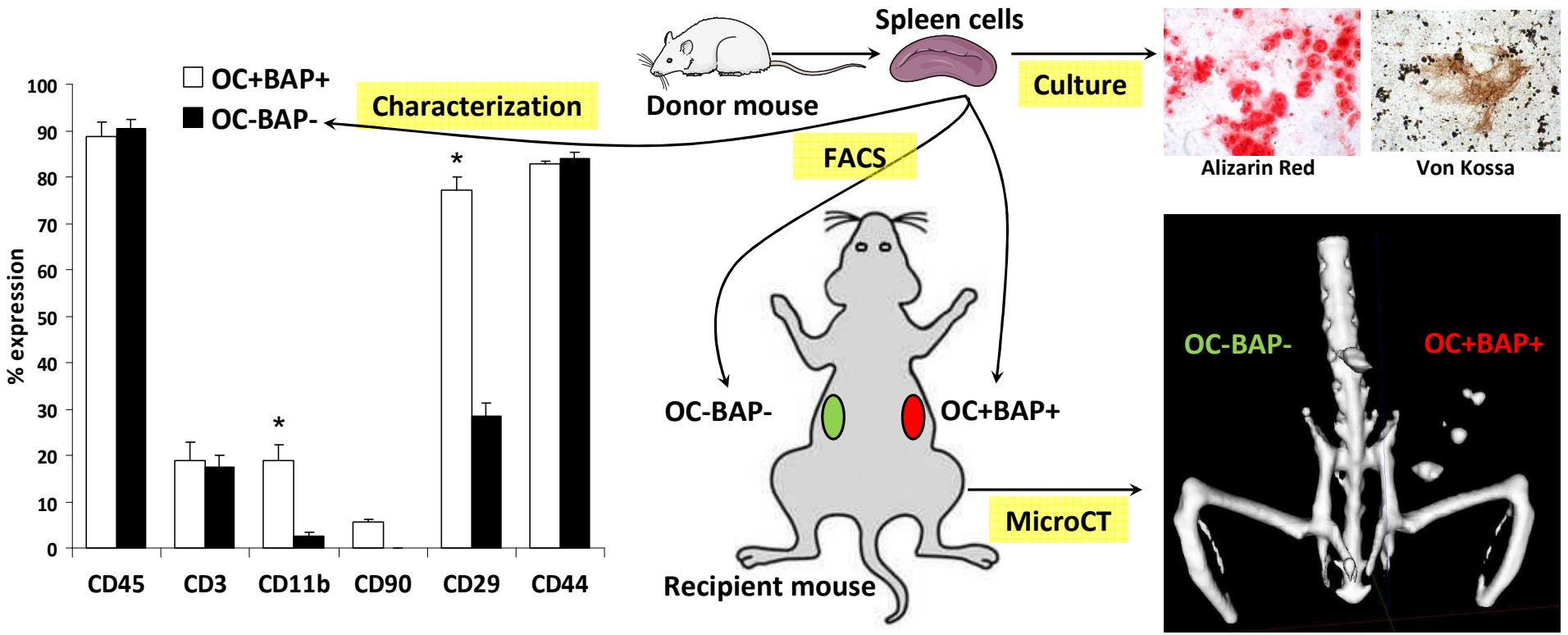
OC+BAP+
OC-BAP-
Characterization
% expression
100
90
80
70
60
50
40
30
20
10
0
CD45
CD3
CD11b
CD90
CD29
CD44
*
*
Donor mouse
Spleen cells
Culture
FACS
Alizarin Red
Von Kossa
OC-BAP-
OC+BAP+
Recipient mouse
MicroCT
OC-BAP-
OC+BAP+

Figure 2

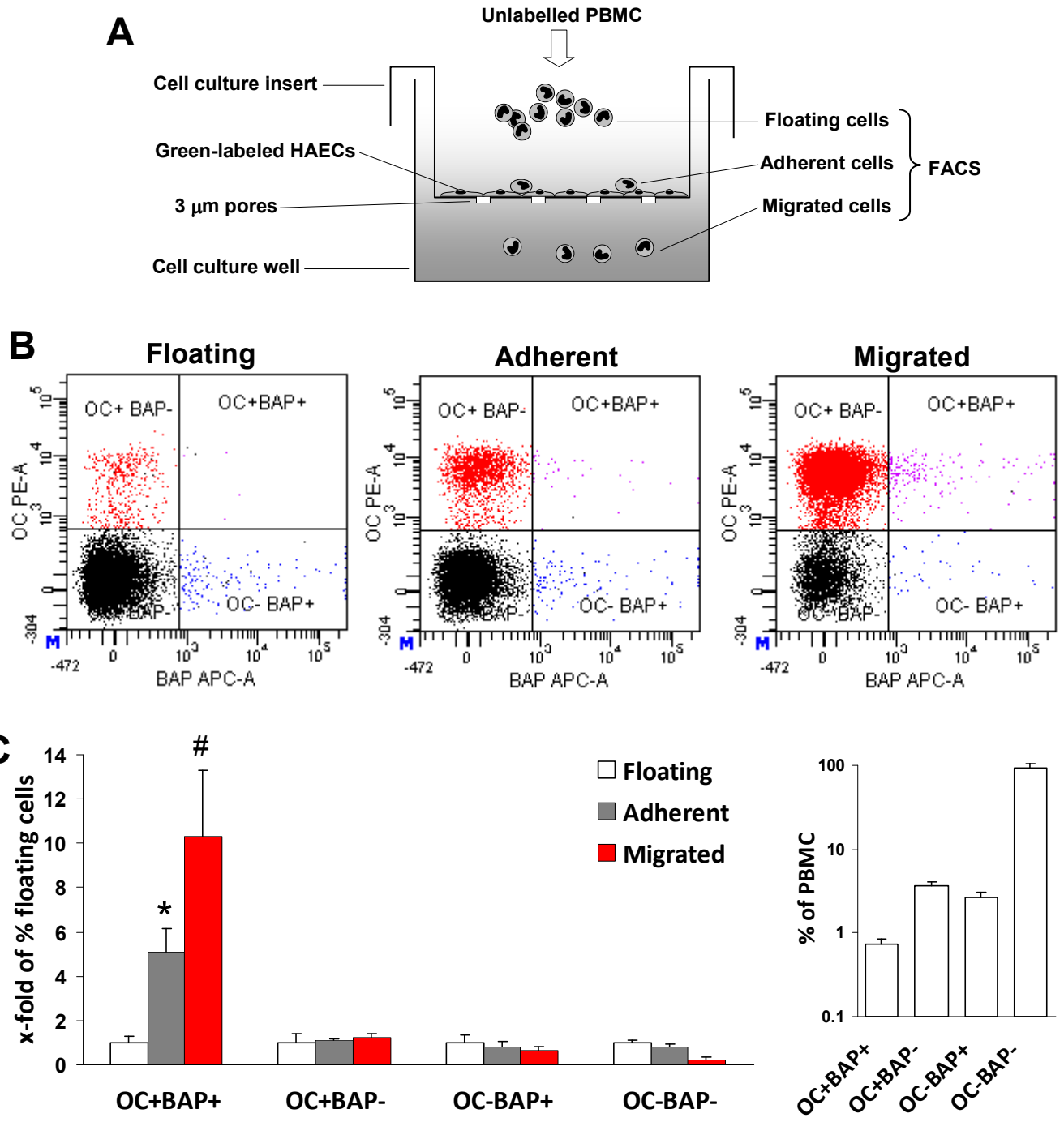
A
Unlabelled PBMC
Cell culture insert
Floating cells
Green-labeled HAECs
Adherent cells
FACS
3 μm pores
Migrated cells
Cell culture well
B
Floating
Adherent
Migrated
OC+ BAP-
OC+BAP+
OC- BAP+
OC PE-A
BAP APC-A
C
x-fold of % floating cells
Floating
Adherent
Migrated
OC+BAP+
OC+BAP-
OC-BAP+
OC-BAP-
% of PBMC

Figure 3

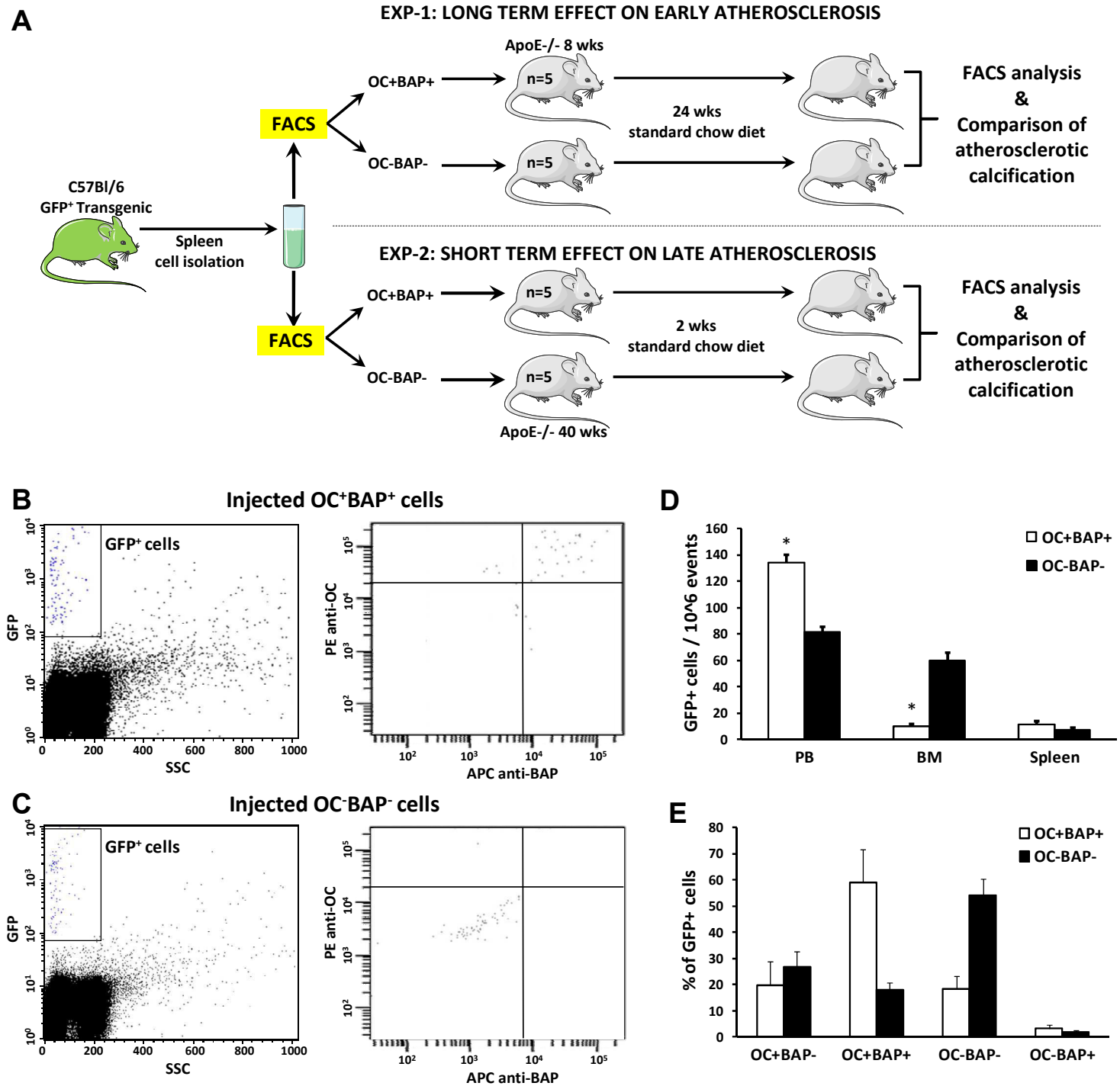
A
EXP-1: LONG TERM EFFECT ON EARLY ATHEROSCLEROSIS
ApoE-/- 8 wks
OC+BAP+
n=5
FACS
OC-BAP-
n=5
24 wks
standard chow diet
FACS analysis
&
Comparison of
atherosclerotic
calcification
C57Bl/6
GFP+ Transgenic
Spleen
cell isolation
EXP-2: SHORT TERM EFFECT ON LATE ATHEROSCLEROSIS
OC+BAP+
n=5
FACS
OC-BAP-
n=5
2 wks
standard chow diet
FACS analysis
&
Comparison of
atherosclerotic
calcification
ApoE-/- 40 wks
B
Injected OC+BAP+ cells
GFP+ cells
GFP
SSC
PE anti-OC
APC anti-BAP
C
Injected OC-BAP- cells
GFP+ cells
GFP
SSC
PE anti-OC
APC anti-BAP
D
GFP+ cells / 10^6 events
OC+BAP+
OC-BAP-
PB
BM
Spleen
E
% of GFP+ cells
OC+BAP+
OC-BAP-
OC+BAP-
OC+BAP+
OC-BAP-
OC-BAP+

Figure 4

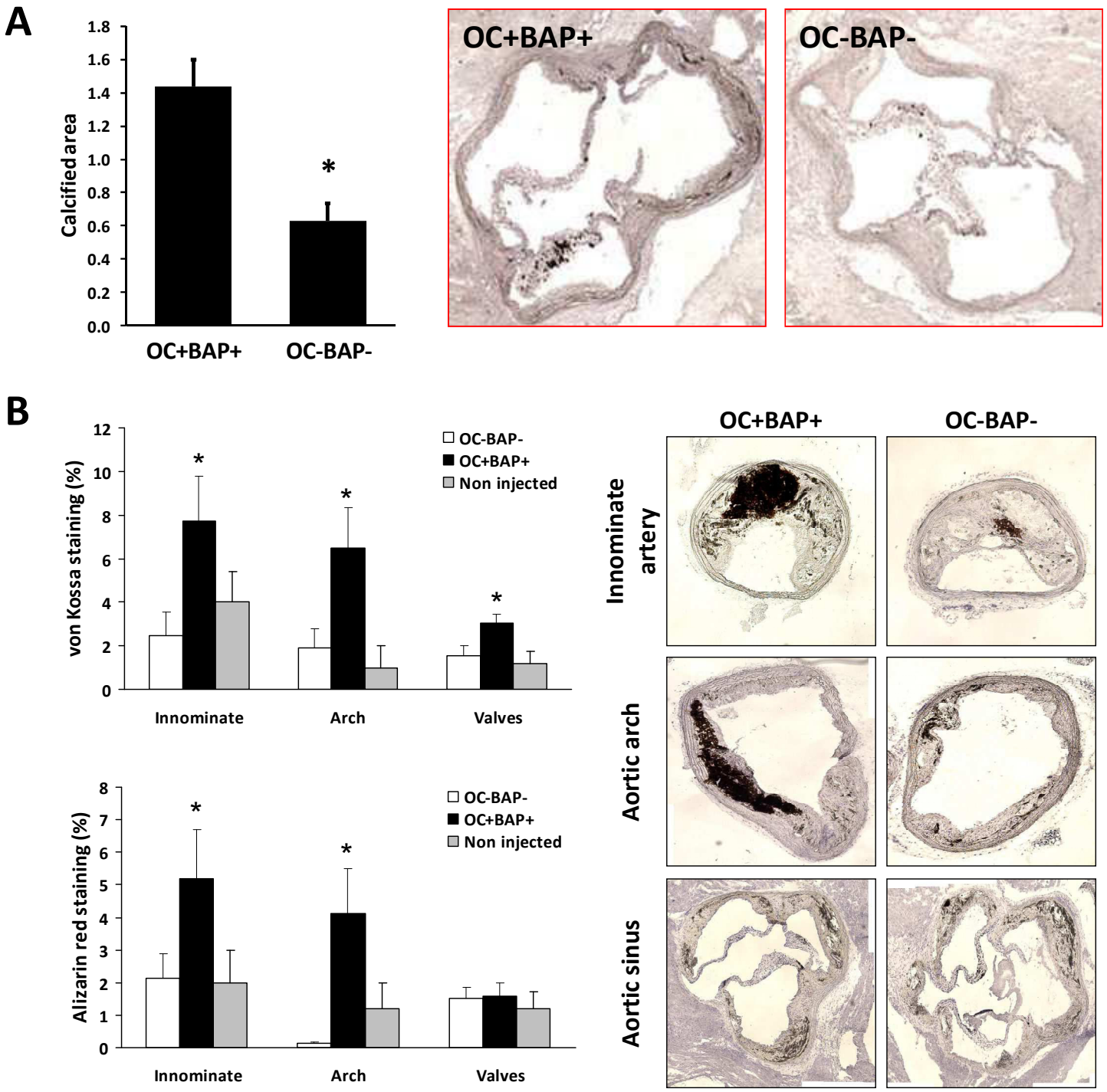
A
Calcified area
1.8
1.6
1.4
1.2
1.0
0.8
0.6
0.4
0.2
0.0
*
OC+BAP+
OC-BAP-
OC+BAP+
OC-BAP-
B
von Kossa staining (%)
12
10
8
6
4
2
0
OC-BAP-
OC+BAP+
Non injected
*
*
*
Innominate
Arch
Valves
Alizarin red staining (%)
8
7
6
5
4
3
2
1
0
OC-BAP-
OC+BAP+
Non injected
*
*
Innominate
Arch
Valves
OC+BAP+
OC-BAP-
Innominate artery
Aortic arch
Aortic sinus

Figure 5

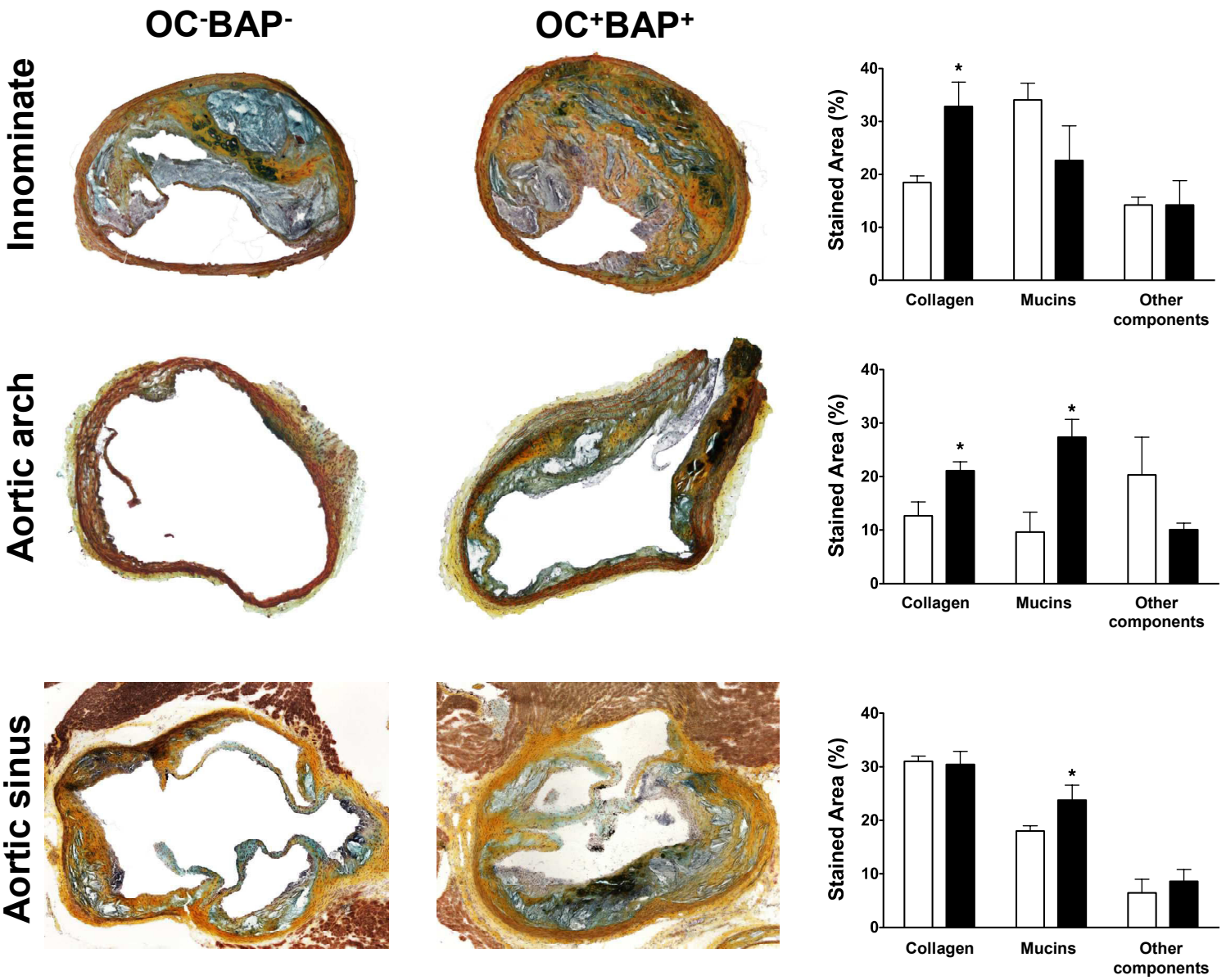
OC-BAP-
OC+BAP+
Innominate
Aortic arch
Aortic sinus
Stained Area (%)
40
30
20
10
0
*
Collagen
Mucins
Other components

Figure 6

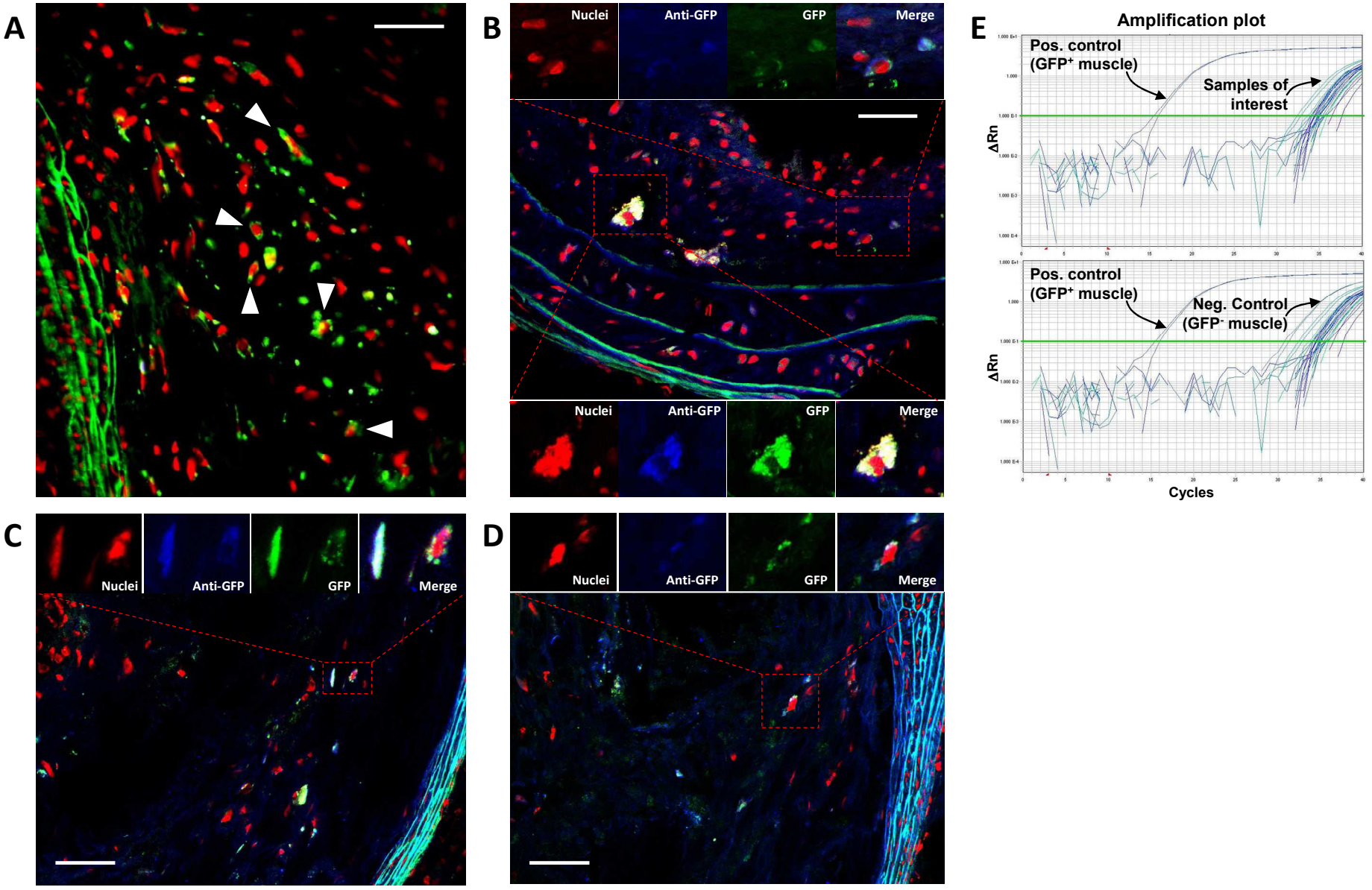
A
B
Nuclei
Anti-GFP
GFP
Merge
C
D
E
Amplification plot
Pos. control
(GFP+ muscle)
Samples of
interest
ΔRn
Pos. control
(GFP+ muscle)
Neg. Control
(GFP- muscle)
ΔRn
Cycles

Figure 7

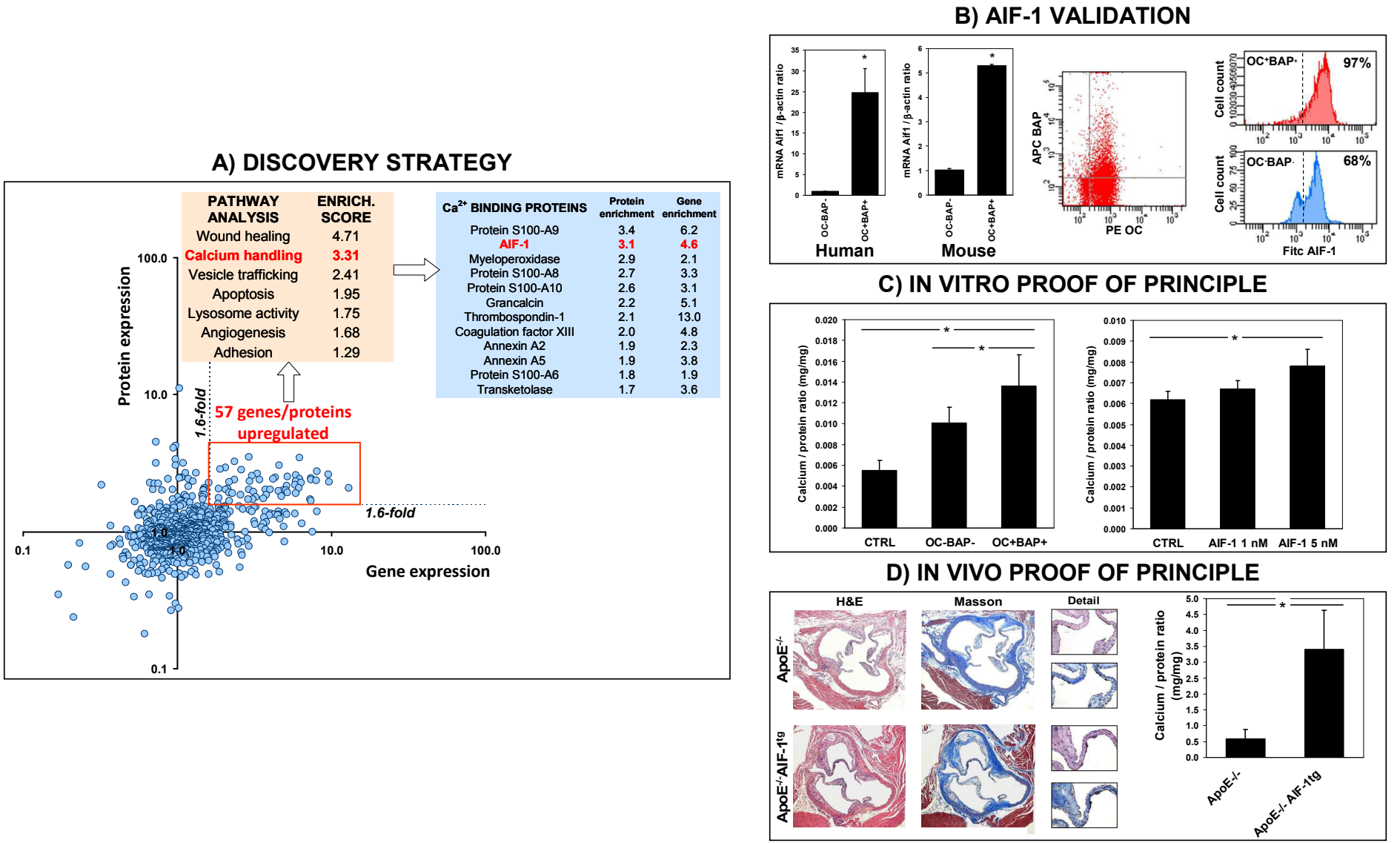
A) DISCOVERY STRATEGY
PATHWAY ANALYSIS
ENRICH. SCORE
Wound healing 4.71
Calcium handling 3.31
Vesicle trafficking 2.41
Apoptosis 1.95
Lysosome activity 1.75
Angiogenesis 1.68
Adhesion 1.29
Ca2+ BINDING PROTEINS
Protein enrichment
Gene enrichment
Protein S100-A9 3.4 6.2
AIF-1 3.1 4.6
Myeloperoxidase 2.9 2.1
Protein S100-A8 2.7 3.3
Protein S100-A10 2.6 3.1
Grancalcin 2.2 5.1
Thrombospondin-1 2.1 13.0
Coagulation factor XIII 2.0 4.8
Annexin A2 1.9 2.3
Annexin A5 1.9 3.8
Protein S100-A6 1.8 1.9
Transketolase 1.7 3.6
57 genes/proteins upregulated
1.6-fold
Protein expression
Gene expression
100.0
10.0
1.0
0.1
B) AIF-1 VALIDATION
mRNA Aif1 /β-actin ratio
OC-BAP-
OC+BAP+
Human
Mouse
APC BAP
PE OC
Cell count
OC+BAP+ 97%
OC-BAP- 68%
Fitc AIF-1
C) IN VITRO PROOF OF PRINCIPLE
Calcium / protein ratio (mg/mg)
CTRL
OC-BAP-
OC+BAP+
AIF-1 1 nM
AIF-1 5 nM
D) IN VIVO PROOF OF PRINCIPLE
H&E
Masson
Detail
ApoE-/-
ApoE-/-AIF-1tg
Calcium / protein ratio (mg/mg)

Uniprot ID	Gene ID	Description	Protein enrichment	Gene enrichment
P08670	7431	Vimentin OS=Homo sapiens GN=VIM PE=1 SV=4 - [VIME_HUMAN]	3.482238179	2.930761841
P06702	6280	Protein S100-A9 OS=Homo sapiens GN=S100A9 PE=1 SV=1 - [S10A9_HUMAN]	3.447432623	6.192923044
P52209	5226	6-phosphogluconate dehydrogenase, decarboxylating OS=Homo sapiens GN=PGD PE=1 SV=3 - [6PGD_HU	3.226353428	2.360113683
P55008	**199**	**Allograft inflammatory factor 1 OS=Homo sapiens GN=AIF1 PE=1 SV=1 - [AIF1_HUMAN]**	**3.053542225**	**4.613849631**
P05164	4353	Isoform H14 of Myeloperoxidase OS=Homo sapiens GN=MPO - [PERM_HUMAN]	2.947806291	2.055420623
Q01469	2171	Fatty acid-binding protein, epidermal OS=Homo sapiens GN=FABP5 PE=1 SV=3 - [FABP5_HUMAN]	2.855224467	1.892795612
Q9UBR2	1522	Cathepsin Z OS=Homo sapiens GN=CTSZ PE=1 SV=1 - [CATZ_HUMAN]	2.817810665	2.602898311
Q96QH2	84106	PML-RARA-regulated adapter molecule 1 OS=Homo sapiens GN=PRAM1 PE=1 SV=2 - [PRAM_HUMAN]	2.754025666	8.057007381
P05109	6279	Protein S100-A8 OS=Homo sapiens GN=S100A8 PE=1 SV=1 - [S10A8_HUMAN]	2.65451622	3.299429455
Q10588	683	ADP-ribosyl cyclase 2 OS=Homo sapiens GN=BST1 PE=1 SV=2 - [BST1_HUMAN]	2.62924268	9.567197008
P23141	1066	Liver carboxylesterase 1 OS=Homo sapiens GN=CES1 PE=1 SV=2 - [EST1_HUMAN]	2.566576887	5.883519836
P60903	6281	Protein S100-A10 OS=Homo sapiens GN=S100A10 PE=1 SV=2 - [S10AA_HUMAN]	2.56093783	3.057574286
Q96CX2	115207	BTB/POZ domain-containing protein KCTD12 OS=Homo sapiens GN=KCTD12 PE=1 SV=1 - [KCD12_HUMA	2.521254741	5.212325072
P40121	822	Macrophage-capping protein OS=Homo sapiens GN=CAPG PE=1 SV=2 - [CAPG_HUMAN]	2.494215503	4.321403367
P08571	929	Monocyte differentiation antigen CD14 OS=Homo sapiens GN=CD14 PE=1 SV=2 - [CD14_HUMAN]	2.457310215	7.370190536
P16671	948	Platelet glycoprotein 4 OS=Homo sapiens GN=CD36 PE=1 SV=2 - [CD36_HUMAN]	2.437113479	6.231152034
P04839	1536	Cytochrome b-245 heavy chain OS=Homo sapiens GN=CYBB PE=1 SV=2 - [CY24B_HUMAN]	2.411794673	4.173676671
P80723	10409	Isoform 2 of Brain acid soluble protein 1 OS=Homo sapiens GN=BASP1 - [BASP1_HUMAN]	2.405743709	7.384046173
O75367	9555	Isoform 3 of Core histone macro-H2A.1 OS=Homo sapiens GN=H2AFY - [H2AY_HUMAN]	2.401394175	2.369266728
Q16555	1808	Dihydropyrimidinase-related protein 2 OS=Homo sapiens GN=DPYSL2 PE=1 SV=1 - [DPYL2_HUMAN]	2.396817943	3.415912987
P19878	4688	Neutrophil cytosol factor 2 OS=Homo sapiens GN=NCF2 PE=1 SV=2 - [NCF2_HUMAN]	2.374384459	7.997698158
P41218	4332	Myeloid cell nuclear differentiation antigen OS=Homo sapiens GN=MNDA PE=1 SV=1 - [MNDA_HUMAN]	2.343842135	5.874886151
P09382	3956	Galectin-1 OS=Homo sapiens GN=LGALS1 PE=1 SV=2 - [LEG1_HUMAN]	2.32453854	2.955172624
P09601	3162	Heme oxygenase 1 OS=Homo sapiens GN=HMOX1 PE=1 SV=1 - [HMOX1_HUMAN]	2.316324242	9.682357243
O75874	3417	Isocitrate dehydrogenase [NADP] cytoplasmic OS=Homo sapiens GN=IDH1 PE=1 SV=2 - [IDHC_HUMAN]	2.308540853	2.189173419
Q92820	8836	Gamma-glutamyl hydrolase OS=Homo sapiens GN=GGH PE=1 SV=2 - [GGH_HUMAN]	2.277618507	1.61515662
P05091	217	Aldehyde dehydrogenase, mitochondrial OS=Homo sapiens GN=ALDH2 PE=1 SV=2 - [ALDH2_HUMAN]	2.267819674	6.399892557
P23381	7453	Tryptophan--tRNA ligase, cytoplasmic OS=Homo sapiens GN=WARS PE=1 SV=2 - [SYWC_HUMAN]	2.200042769	5.822516788
P28676	25801	Grancalcin OS=Homo sapiens GN=GCA PE=1 SV=2 - [GRAN_HUMAN]	2.171101183	5.120882187
P09467	2203	Fructose-1,6-bisphosphatase 1 OS=Homo sapiens GN=FBP1 PE=1 SV=5 - [F16P1_HUMAN]	2.076504863	6.170451494
P07996	7057	Thrombospondin-1 OS=Homo sapiens GN=THBS1 PE=1 SV=2 - [TSP1_HUMAN]	2.067858348	13.02830043
Q0VD83	55911	Isoform 3 of Apolipoprotein B receptor OS=Homo sapiens GN=APOBR - [APOBR_HUMAN]	2.061568243	1.868535471
P04040	847	Catalase OS=Homo sapiens GN=CAT PE=1 SV=3 - [CATA_HUMAN]	2.058346879	2.126221241
A8MVU1	654817	Putative neutrophil cytosol factor 1C OS=Homo sapiens GN=NCF1C PE=5 SV=1 - [NCF1C_HUMAN]	2.037676042	3.736553538
P13473	3920	Lysosome-associated membrane glycoprotein 2 OS=Homo sapiens GN=LAMP2 PE=1 SV=2 - [LAMP2_HUM	2.027927785	4.021809165
P16070	960	Isoform 12 of CD44 antigen OS=Homo sapiens GN=CD44 - [CD44_HUMAN]	2.027501763	2.048521232
Q15942	7791	Zyxin OS=Homo sapiens GN=ZYX PE=1 SV=1 - [ZYX_HUMAN]	2.023041452	2.919039426
P00488	2162	Coagulation factor XIII A chain OS=Homo sapiens GN=F13A1 PE=1 SV=4 - [F13A_HUMAN]	2.011620491	4.828926446
P17931	3958	Galectin-3 OS=Homo sapiens GN=LGALS3 PE=1 SV=5 - [LEG3_HUMAN]	2.001404443	5.092891706
Q9ULZ3	29108	Isoform 3 of Apoptosis-associated speck-like protein containing a CARD OS=Homo sapiens GN=PYCARD -	1.985489104	4.512577854
P50552	7408	Vasodilator-stimulated phosphoprotein OS=Homo sapiens GN=VASP PE=1 SV=3 - [VASP_HUMAN]	1.944804886	3.131708052
P29350	5777	Isoform 3 of Tyrosine-protein phosphatase non-receptor type 6 OS=Homo sapiens GN=PTPN6 - [PTN6_HUM	1.936628883	2.182771114
Q9ULV4	23603	Coronin-1C OS=Homo sapiens GN=CORO1C PE=1 SV=1 - [COR1C_HUMAN]	1.916972767	5.2241182
P07355	302	Annexin A2 OS=Homo sapiens GN=ANXA2 PE=1 SV=2 - [ANXA2_HUMAN]	1.907689604	2.289374654
P19971	1890	Thymidine phosphorylase OS=Homo sapiens GN=TYMP PE=1 SV=2 - [TYPH_HUMAN]	1.899774455	5.858781872
P38606	523	V-type proton ATPase catalytic subunit A OS=Homo sapiens GN=ATP6V1A PE=1 SV=2 - [VATA_HUMAN]	1.852371108	2.591206106
P08758	308	Annexin A5 OS=Homo sapiens GN=ANXA5 PE=1 SV=2 - [ANXA5_HUMAN]	1.852002829	3.797703389
P07858	1508	Cathepsin B OS=Homo sapiens GN=CTSB PE=1 SV=3 - [CATB_HUMAN]	1.811081517	4.738184226
P62942	2280	Peptidyl-prolyl cis-trans isomerase FKBP1A OS=Homo sapiens GN=FKBP1A PE=1 SV=2 - [FKB1A_HUMAN	1.782836108	3.227615597
P06703	6277	Protein S100-A6 OS=Homo sapiens GN=S100A6 PE=1 SV=1 - [S10A6_HUMAN]	1.76927793	1.862373176
P29401	7086	Transketolase OS=Homo sapiens GN=TKT PE=1 SV=3 - [TKT_HUMAN]	1.741792972	3.639468143
P13284	10437	Gamma-interferon-inducible lysosomal thiol reductase OS=Homo sapiens GN=IFI30 PE=1 SV=3 - [GILT_HU	1.726063963	7.283362887
P09211	2950	Glutathione S-transferase P OS=Homo sapiens GN=GSTP1 PE=1 SV=2 - [GSTP1_HUMAN]	1.720518208	3.077989843
P10619	5476	Lysosomal protective protein OS=Homo sapiens GN=CTSA PE=1 SV=2 - [PPGB_HUMAN]	1.711447303	2.901181431
Q6XQN6	93100	Isoform 3 of Nicotinate phosphoribosyltransferase OS=Homo sapiens GN=NAPRT1 - [PNCB_HUMAN]	1.682487653	2.17241285
P52790	3101	Hexokinase-3 OS=Homo sapiens GN=HK3 PE=1 SV=2 - [HXK3_HUMAN]	1.675665794	7.353859678
P06733	2023	Alpha-enolase OS=Homo sapiens GN=ENO1 PE=1 SV=2 - [ENOA_HUMAN]	1.60248863	1.847594767